

RESEARCH

Open Access



Bidirectional roles of nanoenzymes in enhancing GPC3-CAR T cell infiltration and cancer immunotherapy

Yu Xu^{1,2†}, Jianping Liao^{1,2,3†}, Jiahong Wang^{1,2†}, Yuan Gao^{1,2†}, Yuan Wu^{1,2}, Meiqin Gao¹, Wenwen Liu¹, Da Zhang^{1,2,5}, Wenmin Zhang^{1,2,4} and Aimin Huang^{1,2*}

Abstract

Background Vascular abnormalities and hypoxia in solid tumors limit the efficacy of chimeric antigen receptor (CAR) T-cell therapy. This study proposes a biomimic nanoenzyme, Lenv@BSA-PtNPs, combining platinum nanoparticles (PtNPs) and lenvatinib, to address these challenges in a hepatocellular carcinoma (HCC) nonobese diabetic (NOD) mice model.

Methods Lenv@BSA-PtNPs were designed using albumin as a solubilizer, embedding lenvatinib via hydrophobic interactions and facilitating in situ PtNPs generation. The nanoenzyme functions as a catalase, converting H₂O₂ to O₂, downregulating hypoxia-inducible factor (HIF-1), and normalizing tumor vasculature. Its efficacy was evaluated in a glypican-3 (GPC3)-CAR T-cell therapy model for HCC.

Results Lenv@BSA-PtNPs significantly improved tumor oxygenation, normalized vasculature, and enhanced GPC3-CAR T-cell infiltration into tumors. This led to potent antitumor effects and prolonged survival in the HCC mouse model.

Conclusions Lenv@BSA-PtNPs provide a simple and effective strategy to enhance CAR-T cell accumulation and efficacy by ameliorating hypoxia and normalizing tumor vasculature, offering a promising approach for improving CAR-T therapy in solid tumors.

Keywords Nanoenzyme, Vascular normalization, Hypoxia, GPC3-CAR T cells immunity

[†]Yu Xu, Jianping Liao, Jiahong Wang and Yuan Gao contributed equally to this work.

*Correspondence:

Aimin Huang
aimin@fjmu.edu.cn

¹Department of Pathology, School of Basic Medical Sciences, Fujian Medical University, 88 Jiaotong Road, Fuzhou 350004, Fujian, China

²Institute of Oncology, Fujian Medical University, 88 Jiaotong Road, Fuzhou 350004, Fujian, China

³Department of Medical Oncology, State Key Laboratory of Oncology in South China, Collaborative Innovation Center for Cancer Medicine, Sun Yat-sen University Cancer Center, Sun Yat-sen University, Guangzhou 510060, P. R. China

⁴Diagnosical Pathology Center, Fujian Medical University, Fuzhou 350004, Fujian, China

⁵The United Innovation of Mengchao Hepatobiliary Technology Key Laboratory of Fujian Province, Mengchao Hepatobiliary Hospital of Fujian Medical University, Fuzhou 350025, P. R. China



Introduction

Since the initial success of anti-CD19 chimeric antigen receptor (CAR) T cell therapy in pre-B cell acute lymphoblastic leukemia (ALL) or B cell lymphomas and its subsequent food and drug administration (FDA) approval [1], this approach has emerged as a promising immunotherapy for hematological cancers [2, 3]. While over 100 clinical trials are currently investigating CAR T cell therapies globally, their long-term clinical impact remains under evaluation. Current data indicate that anti-CD19 CAR T cells achieve objective responses in 30–50% of patients with ALL or B-cell lymphomas [4], though relapse within one year remains a significant challenge [5]. Furthermore, efficacy in solid tumors—such as hepatocellular carcinoma—has been limited [6–9], in part due to poor immune effector cells infiltration [10, 11]. Additionally, abnormal vessels and insufficient blood circulation create a hypoxic tumor microenvironment (TME) that further diminishes the immune response against cancer cells [12, 13].

Hypoxia reprograms CAR T cell metabolism via activation of hypoxia-inducible factor 1- α (HIF-1 α), suppressing oxidative phosphorylation while promoting glycolysis, ultimately impairing effector function [14]. HIF-1 α accumulation under low oxygen conditions drives T cell differentiation toward a terminally exhausted state and downregulates key effector genes such as IFN- γ [15]. In addition, hypoxia induces the expression of immunosuppressive molecules like PD-L1 [16], further accelerating CAR T cell exhaustion. Disorganized tumor vasculature—characterized by increased leakiness and dysfunctional pericyte support—elevates interstitial fluid pressure, thereby hindering CAR T cell infiltration [17]. Chronic hypoxia, a consequence of aberrant vasculature, drives the release of immunosuppressive factors such as VEGF and adenosine, dampening CAR T cell metabolic activity [18]. VEGF overexpression not only suppresses T cell function directly but also facilitates regulatory T cell (Treg) infiltration. Moreover, hypoxia-induced HIF-1 α upregulates VEGF, perpetuating vascular dysfunction and immune evasion—a feed forward loop referred to as the “hypoxia–angiogenesis–immunosuppression” axis. These limitations highlight the need for strategies to enhance CAR T cell delivery and potency, which are now key focuses of ongoing research.

Recently, nanoenzymes with biomimetic enzyme properties have been shown to modulate the TME and enhance cancer immunotherapy by improving hypoxia [19, 20], reducing redox status [21], and degrading immunosuppressive molecules in the TME [22]. Compared with natural bioenzymes (e.g., glucose oxidase and sialidase), nanoenzymes offer several advantages, including smaller size, higher stability, lower cost, and better tumor penetration and accumulation. Numerous nanozymes

(e.g., Fe₃O₄, cerium oxide, Mn₃O₄, PtNPs, and RNA-cleaving DNazymes) have been developed since the discovery of the first nanozyme (GNPs) in 2004 [23–25]. To date, most nanozymes act as Fenton-like agents, inducing immunogenic cell death (ICD) by catalyzing TME substrates to elicit immunity or modulating the immunosuppressive TME to enhance immune response [26–28]. Nevertheless, the chemical engineering of bidirectional functions of nanoenzymes to normalize tumor vasculature and ameliorate hypoxia for enhancing CAR T cell therapy *in vivo* has not been well investigated.

In this study, a platinum nanoparticle (PtNP) and lenvatinib-based biomimetic nanoenzyme was developed to ameliorate hypoxia and normalize tumor vessels, thereby enhancing the antitumor efficacy of GPC3-CAR T cell therapy in a hepatocellular carcinoma (HCC) model with poor response (Fig. 1A). Lenvatinib, an FDA-approved oral multi-targeted tyrosine kinase inhibitor for unresectable HCC, normalizes abnormal tumor vessels. However, lenvatinib's poor aqueous solubility and undesirable side effects, such as elevated blood pressure, diarrhea, fatigue, and nausea, limit its widespread application in HCC patients. Here, albumin is used as a substrate, embedding lenvatinib via its hydrophobic domain to enhance water solubility. *In situ* generation of PtNPs then forms the biomimetic nanoenzyme, referred to as Lenv@BSA-PtNPs. This nanoenzyme not only catalyzes H₂O₂ to O₂ to improve the hypoxic TME but also remodels tumor vessels to achieve normalization. This enhancement led to increased infiltration of GPC3-CAR T cells in tumors, resulting in significant antitumor efficacy and prolonged survival in established primary tumor models in NOD mice, compared to the intravenous administration of GPC3-CAR T cells or nanoenzyme alone.

Materials and methods

Materials

Lenvatinib was purchased from APEX BIO Technology (Houston, Texas, US). Tris (4, 7-diphenyl-1, 10-phenanthroline) ruthenium (II) dichloride (Ru(dpp)₃Cl₂) and H₂PtCl₆ were purchased from J&K Scientific. 4, 6-Diamidino-2-phenylindole dihydrochloride (DAPI) was purchased from Dojindo Molecular Technologies. Cell Counting Kit (CCK-8) and Live / Dead staining Kit were purchased from Dojindo Laboratories (Kumamoto, Japan). ATP assay Kit were purchased from Beyotime Biotechnology (Shanghai, China). ELISA kits purchased from Fankewei (Shanghai, China) were obtained to detect the IL-2, IFN γ . Unless specified, all other chemicals were commercially available and used as received.

Cell lines and culture

The human HCC cell lines SK-HEP-1, Hep3B, hepatoblastoma cell line HepG2, and HEK-293T were purchased

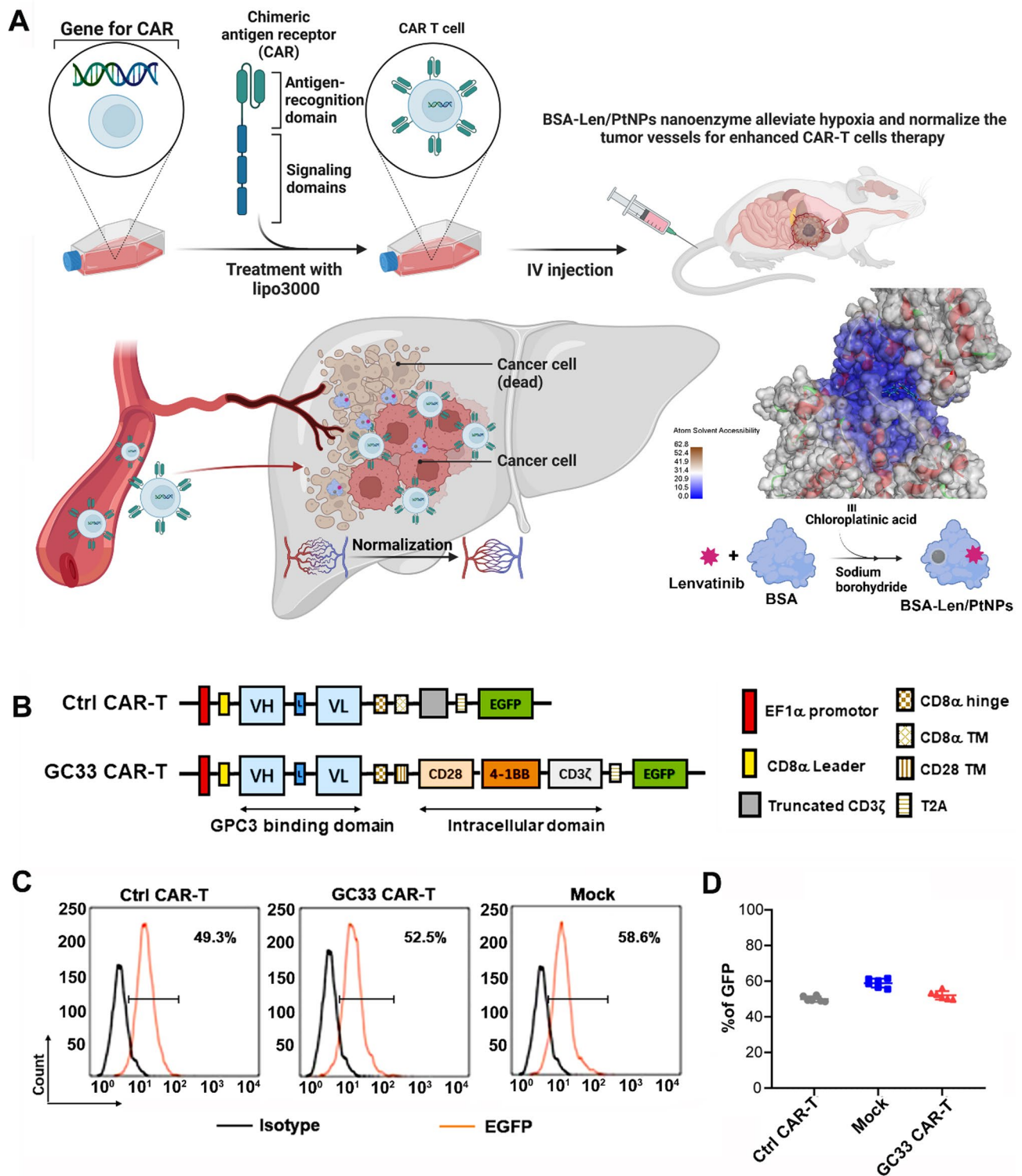


Fig. 1 Creating a CART cell specifically targeting GPC3. **(A)** Schematic illustration of the preparation of bidirectional roles of BSA-Len/PtNPs to ameliorate hypoxia and normalize vessels of tumors for enhancing antitumor efficiency of GPC3-CAR T cells in a poorly responsive hepatocellular carcinoma NOD mice model. **(B)** Schematic structure of Ctrl CAR-T and GC33 CAR-T. **(C)** The transduction efficiency of Ctrl CAR-T, GC33 CAR-T and Mock groups. **(D)** The percentage of GFP-positive cells in C. All data were subjected to at least three separate experiments

from the American Type Culture Collection (ATCC, USA). Human HCC cell lines HL7702, and Huh7 were purchased from the Chinese Cell Bank of the Chinese Academy of Sciences (Shanghai, China). SMMC7721 was purchased from the cell bank of the Shanghai Institute of Cell Biology (Shanghai, China). Huh-7-KO cell line was generated from Huh-7 cells by genetically knocking out the GPC3 gene using pU6gRNACas9 vector (GenePharma, Shanghai, China). Huh-7 cell lines were transduced with a lentiviral vector encoding the luciferase reporter gene to generate the Huh-7-luc cell line. The HL7702 cell line was maintained in RPMI-1640 (HyClone, USA). All other cells were cultured in DMEM (Gibco, USA). Both media were supplemented with 10% heat-inactivated fetal bovine serum (FBS; Gibco, USA), and the cells were incubated in a humidified incubator with 5% CO₂ at 37°C and passaged every 2 days with a complete culture medium change. Mycoplasma infection was verified by the specific PCR assay using MycoBlue Mycoplasma Detector Kit (#D101-01, Vazyme).

Mice

NCG mice (NOD-Prkdcem26Cd52Il2rgem26Cd22/Nju) and were purchased from Model Animal Resource Information Platform of Nanjing University. Six to eight weeks of age female mice were maintained under specific pathogen-free facilities with a 12-h light/dark cycle and had free access to food and water at Fujian Medical University. All surgical procedures were performed under aseptic conditions with 2% pentobarbital anesthesia. At the end of the experiment, the mice were euthanized by an overdose of pentobarbital. All animal experiments were conducted in accordance with NIH guidelines and were approved by the Institutional Animal Care and Use Committees of Fujian Medical University.

Preparation of BSA-Len/PtNPs nanozyme

The BSA-Len/PtNPs was prepared using previously established methods with slight modifications [29, 30]. Typically, to prepare the lenvatinib-based BSA-PtNPs (BSA-Len/PtNPs), an aqueous solution of BSA (5 mg/mL) was mixed with lenvatinib (0.5 mg, DMSO) for shaking 12 h. Afterward, the mixture was purified by ultrafiltration (3KDa) through Di-water for 3 times. The obtained Lb-BSA (5 mg/mL, BSA) was mixed with H₂PtCl₆ (0.5 mg) and NaOH (2 M, 0.1 mL) in a water bath heated to 80°C and reaction for 2.5 h. Afterward, the production of BSA-Len/PtNPs was then purified through ultrafiltration (3KDa). Afterward, the quantification of lenvatinib was measured by absorbance of lenvatinib at 320 nm from BSA-Len/PtNPs in DMSO. The standard curve at 320 nm with good linear correlation from 0~1.2 mg/mL was obtained ($Y=2.0583x+0.3686$,

$R^2=0.99$). Therefore, the lenvatinib in BSA-Len/PtNPs (5 mg/mL) was determined to be 0.214 mg/mL.

Construction of the GPC3 targeted CAR vectors

To generate GPC3 targeted CARs, GPC3 CAR (third generation) was constructed by linking the anti-GPC3 scFv (based on GC33 antibodies) to a hinge and transmembrane domain of CD8, followed by an intracellular domain of CD28, incorporating another co-stimulatory intracellular domain of 4-1BB and an intracellular domain of CD3ζ. The sequence of each cloned CAR was verified *via* sequencing. CAR linked with a truncated form of the CD3ζ intracellular domain lacking signal transduction was designed as a control. Control and GC33-CARs were further linked to the reporter-enhanced green fluorescence protein (EGFP) with a T2A oligopeptide, respectively. All the CAR cassettes were subsequently subcloned to the lentiviral vector (pLVX-EF1alpha-IRES-ZsGreen1, Takara).

Production of lentivirus and T cell transduction

The GC33-CAR lentivirus particles were produced by co-transfected into HEK293T cells with corresponding CAR-expressing plasmids and three packaging plasmids REV, RRE, and VSVG on a 3:1:1:1 ratio using Lipofectamine 3000 (Thermo Fisher Scientific, L3000015). The medium was changed after 12 h. Lentivirus-containing culture medium were collected at 48 h and 72 h post-transfection and centrifuged at 2000 g for 15 min to remove cell debris. The supernatants were further filtered through 0.22 mm polyvinylidene fluoride filters (Millipore, USA) and concentrated 30-fold by ultracentrifuging at 30,000 g for 2 h (Beckman Optima XPN100, Beckman). Subsequently, the lentivirus particles were re-suspended in appropriate volume using AIM-V medium (Gibco, USA) at 4 °C overnight. Final viral samples were titrated and stored at -80 °C in single-use aliquots.

Buffy coat collected from healthy adult volunteers was obtained from Fujian Blood Center under consent, and was used for isolation of PBMCs. The study was approved by the Committee for the Ethical Review of Research, Fujian Medical University (No. 2018-38). Primary human T cells were isolated from PBMCs using the Pan T Cell Isolation kit human (Miltenyi Biotec, Germany). Freshly isolated T cells were cultured in AIM-V medium (Gibco, USA) supplemented with 10% FBS (FBS; Gibco, USA) and 300 U/mL recombinant human interleukin 2 (rhIL-2) (Jiangsu Jinsili Pharmaceutical, China). These cells were pre-stimulated with anti-CD3/CD28 beads (Thermo Fisher Scientific, 11131D) (1:1 bead-to-cell ratio) for 48 h and transduced with indicated lentivirus particles coated on the non-tissue culture plates with 1 μL/mL polybrene (Santa Cruz, sc-134220). The transduced T cells were cultured at a concentration of

5×10^5 cells/mL in the presence of rhIL-2 (300 U/mL). Transduction efficiency was evaluated by flow cytometry 1 week later.

Flow cytometry and antibodies

To determine GPC3 expression on the surface of HCC cells, the cells were trypsinized into single-cell suspensions and then incubated with anti-glypican-3 antibody (ab207080) (red) or rabbit IgG, monoclonal (EPR25A)-Isotype control (ab172730) (black) at 1/500 dilution. The donkey anti-rabbit IgG H&L (AlexaFluor® 647) was used as a secondary antibody at 1/100 dilution. To evaluate CAR expression, CAR-T cells were washed and incubated with goat anti-human anti-Fab antibody (Jackson ImmunoResearch Inc., FITC-conjugated), at 1:100 dilution. Flow cytometry was performed using a BD FACS Calibur flow cytometer and an LSRII flow cytometer (BD), and results were processed with the Flowjo 7.6.1 software (TreeStar).

Western blot analysis

Cell lysates were harvested and centrifuged for 10 min at 13,000 rpm, 4 °C. Proteins were separated on 10% SDS-PAGE gels and transferred to nitrocellulose membranes. Membranes were probed overnight at 4 °C for anti-glypican-3 (1:500, abcam). Following washes with TBST, membranes were incubated for 1 h at RT with the HRP-labeled secondary antibody (goat anti-rabbit IgG, 1:5000).

RT-qPCR analysis of GPC3 expression

The mRNA expression of GPC3 from different HCC cell lines was detected by RT-qPCR assays. Total RNA was extracted using TransZol reagents (TransGen Biotech, Beijing, China). Briefly, reverse transcription was carried out using Transcriptor First Strand cDNA Synthesis Kit (Roche, Indianapolis, IN, USA) according to the manufacturer's instructions. All reactions were performed with TransStart Tip Green qPCR SuperMix (TransGene, Beijing, China) on a Bio-Rad CFX96 real-time PCR machine (Bio-Rad, Hercules, CA, USA). Real-time PCR determination was performed with the following parameters: 45 cycles of 95 °C for 15 s and 60 °C for 60 s. The relative gene expression of GPC3 was normalized with the reference gene 18 S rRNA, and calculated according to the Livak method ($2^{-\Delta\Delta Ct}$). Specific primers (human GPC3 forward primer sequence—CCTGGAGGAAGACAACACCGCGTGCGCACCGCGTGCTTG; reverse primer sequence—GTGTCCGGAAGACTAAAACCTCCTTCTTCCAGAGACTGC CG; human 18 S rRNA, forward primer sequence—AGAAACGGCTACCACATCCA, and reverse primer sequence —CACCAGACTTGCCCTC

CA-3) were verified with PCR amplification efficiency, which ranked between 90% and 110%.

Cytotoxicity assays

In vitro cytotoxicity assays were performed by incubating control CAR-T, GC33 CAR-T cells or Mock with 0.5 μM CellTrace FarRed (Invitrogen, C34564)-labeled target cells (HepG2, Huh7, Hep3B, SK-HEP-1, PLC/PRF/5, Huh-7-KO) at the different effector: target ratios of 5:1, 1:1, and 1:5 for 18 h. Then, 0.01 mg/mL DAPI (Sigma Aldrich, D8417) was added to each reaction, and the cells were immediately analyzed by flow cytometry within 10s. The % cell lysis was calculated as follows: $[(\text{FarRed} + \text{DAPI} + \text{cells} - \text{spontaneous apoptosis}) / \text{total FarRed} + \text{cells}] \times 100\%$.

Cytokine release assay

Cytokine-releasing assays were performed by co-culturing various genetically modified T cells with different HCC cells for 24 h at the effector/target ratio of 10:1. Supernatants were collected and stored at -80 °C until been measured using a standard ELISA kit (Boster Biotechnology, China) according to the manufacturer's instructions. In vivo cytokine levels of IL-2 and IFN-gamma in the blood were determined using the Human Th1/Th2 Cytokine Kit II (BD Biosciences) following the manufacturer's instructions.

Tumor models and treatments

Cell preparation. Human HCC cell line Huh7 transduced with a lentiviral vector encoding the luciferase reporter gene (Huh-7-luc) was used for tumor injection into the liver to establish the orthotopic xenograft model. Huh-7-luc cells (5×10^5) in 20 μl of PBS were mixed with Matrigel (BD Biosciences, Bedford, MA, USA) (mixing ratio of 1:1). Keep the cell suspension on ice.

For the established orthotopic HCC model. The mice were provided with sterilized food and water ad libitum and housed in negative pressure isolators with 12-hour light/dark cycles. Before the tumor implantation, each mouse was anesthetized with 3% isoflurane for induction and 2% for maintenance. The right lobe of the mouse liver was exposed by laparotomy. The surgical area was wiped with alcohol, and then make a 1.0 cm incision with microsurgical scissors and forceps. Mice were orthotopically inoculated with Huh-7-luc cells (5×10^5 cells/mouse) directly under the surface of the right hepatic lobe on day 0. The liver was returned to its original position in the abdominal cavity after confirming hemostasis and monitored for tumor formation. Tumor burdens were monitored weekly using the IVIS system (Caliper IVIS Lumina II, PerkinElmer). Tumor volumes were calculated with the following formula: $V = (\text{length} \times \text{width}^2) / 2$. When the tumor volume was approximately 50-150mm³ (day 7),

mice were randomly allocated into different groups (consisting of $n = 5$ per group).

For the single-drug treatment. On day 8, mice were grouped: (i) saline group, receiving normal saline intravenously at 0.04 or 0.08 or 0.16 mg/kg/day for 14 days; (ii) mice treated with lenvatinib (E7080, ApexBio Technology, USA) at 0.04 or 0.08 or 0.16 mg/kg/day per os for 14 days; (iii) mice treated with BSA-Len/PtNPs intravenously at 0.04 or 0.08 or 0.16 mg/kg/day for 14 days.

For the groups treated with the combined therapy. On day 8, mice were grouped: (i) saline group, receiving normal saline intravenously at 0.08 or 0.16 mg/kg/day for 14 days; (ii) mice treated with lenvatinib (E7080, ApexBio Technology, USA) at 0.08 or 0.16 mg/kg/day per os for 14 days; (iii) mice treated with BSA-Len/PtNPs intravenously at 0.08 or 0.16 mg/kg/day for 14 days followed by the treatments with two doses of intravenous injections of 5×10^6 GC33 CAR-T cells on days 9 and 16 respectively. The mice treated only with saline without the following GC33 CAR-T cells were presented as the control group. Mice were inspected every day and were euthanized when signs of discomfort were detected. Mice with large tumor masses were euthanized early because of humanitarian considerations.

Bioluminescence imaging

Isoflurane-anesthetized animals were imaged using the IVIS system (Caliper IVIS Lumina II, PerkinElmer) followed by the intraperitoneal injection of 150 mg/kg D-luciferin (PerkinElmer). The data were quantified using Living Image software (Caliper Life Sciences).

TUNEL assay

Tumor sections were subjected to TUNEL staining according to the manufacturer's manual (Roche, Germany). Briefly, 20- μ m-thick tumor sections were rinsed in PBS, incubated in Proteinase K for 15 min at room temperature, and then incubated in a TUNEL reaction mixture (50 μ l per section) for 60 min at 37 °C in the dark. After being washed in PBS and mounted with the mounting medium containing DAPI (Solarbio, Beijing, China), these sections were observed under the fluorescence microscope (ZEISS). Three separate sections of each mouse and three non-overlapping 40 \times fields regions were chosen in a random and blinded manner to quantify TUNEL-positive cells.

Histology, immunohistochemistry and morphometric analyses

Mouse tumor tissues from the indicated tumor-bearing mice were harvested and the tissue specimens were fixed with 10% formalin-fixed with formalin, dehydrated with ethanol, and embedded in paraffin. The tissue samples were sliced into 3- μ m-thick continuous

sheets and stained with hematoxylin and eosin (H&E). Immunohistochemical staining was carried out by the streptavidin peroxidase method according to the manufacturer's instructions (Fuzhou Maixin Biotechnology Development Company, China). Samples were then incubated with anti-mouse CD31 (rat polyclonal, ab56299, Abcam), anti-mouse alpha-smooth muscle actin (rabbit polyclonal, ab32575, Abcam), anti-human CD3 (rat polyclonal, ab11089, Abcam) or anti-mouse hypoxia inducible factor-1 subunit alpha (rabbit monoclonal, ab51608, Abcam) antibodies overnight at 4 °C. The samples were washed with PBS and incubated with a horseradish peroxidase (HRP)-conjugated IgG antibody using Catalyzed Signal Amplification System (DAKO, K1500) for staining. Then, the samples were observed, and images were collected with an optical microscope (BX-46; Olympus, Tokyo, Japan). Differences among tumors from GC33 CAR-T, lenvatinib.08 + CAR-T, lenvatinib.0.16 + CAR-T, BSA-Len/PtNPs.08 + CAR-T, BSA-Len/PtNPs.0.16 + CAR-T and saline-treated mice were assessed by unpaired Student's t-test (two-tailed). The data are presented as the mean \pm SD. All statistical tests were evaluated using a level of 0.05. Statistical analysis was carried out with SPSS software, version 22.0 (SPSS, Chicago, IL).

Statistical analysis

Each experiment presented in this report was repeated at least five times. GraphPad Prism Software v.8.0. (GraphPad Software, La Jolla, CA) was used to generate graphs and perform statistical analyses. All data are expressed as means \pm SD. The significant difference was analyzed by the Student's t-test and one-way ANOVA. Kaplan-Meier method was used to calculate the survival rate and Log-rank (Mantel-Cox) test for the different significance. *P*-values are represented as * ($P < 0.05$), ** ($P < 0.01$), *** ($P < 0.001$) and **** ($P < 0.0001$); ns, not significant.

Results

Development of a GPC3-targeted CART cell

To evaluate the anti-tumor efficacy of CAR-T cells within the vascular abnormalities and a hypoxic microenvironment in HCC, we designed a GC33 CAR construct consisting of a glypican-3 (GPC3) binding domain, a CD8 α hinge, and CD28 TM spacer, and intracellular signaling domains from CD28, 4-1BB and TCR ζ chain (Fig. 1B). GPC3 is a membrane protein expressed in over 70% of HCC tumors but not in normal tissues [31]. T cells expressing CAR targeting GPC3 were previously characterized for the targeting specificity and capacity to eliminate GPC3⁺ tumor cells [32, 33]. The transduction efficiency of control CAR-T and GC33 CAR-T cells was confirmed by flow cytometry, and around 50–60% expression of GFP in three groups indicated the

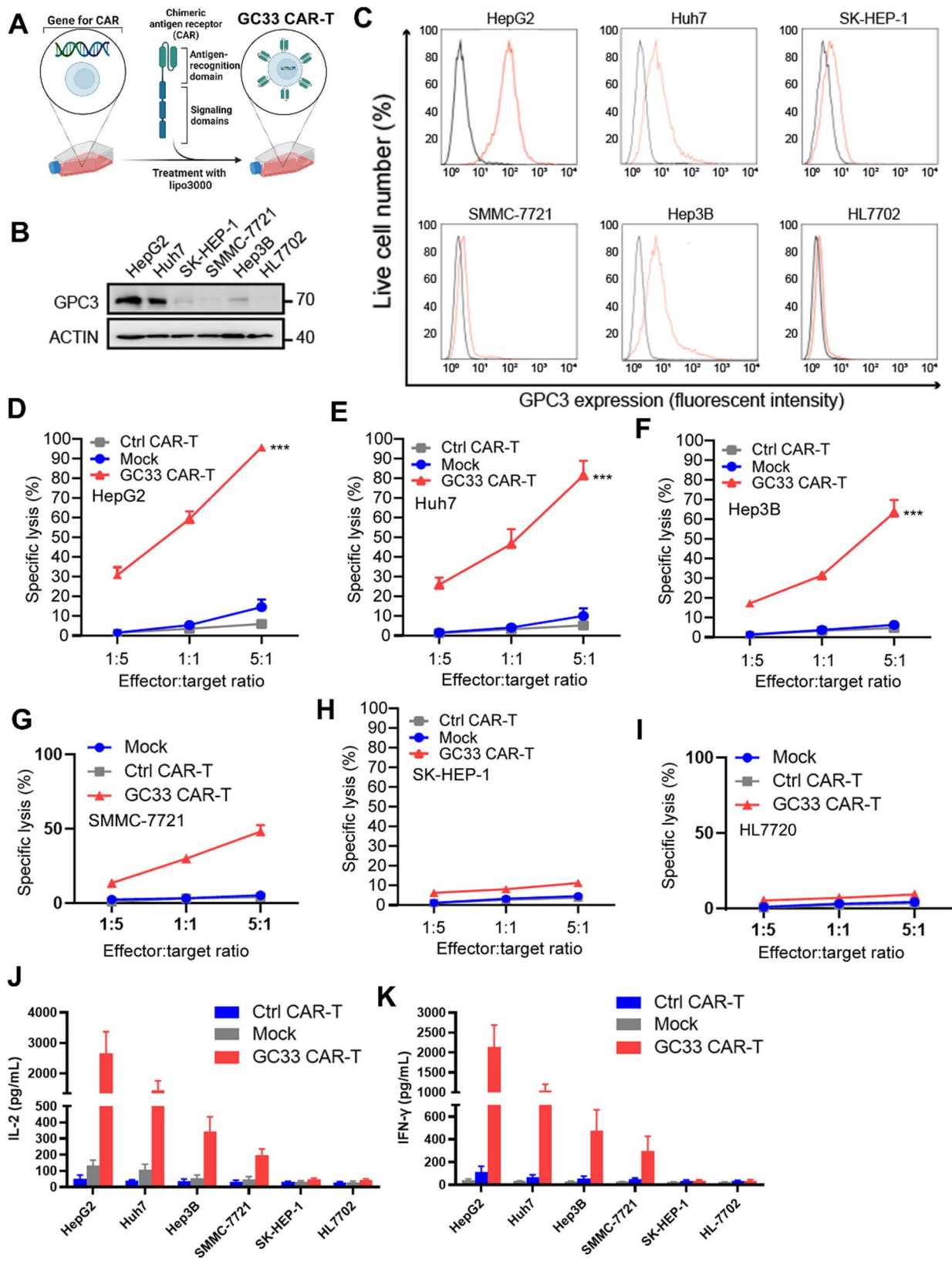


Fig. 2 (See legend on next page.)

(See figure on previous page.)

Fig. 2 GC33 CAR-T-cells selectively target the GPC3⁺ tumor cells. **(A)** Schematic illustration of the preparation of GC33 CAR-T cells. **(B, C)** The expression of GPC3 in six HCC cell lines (HepG2, Huh7, SK-HEP-1, SMMC-7721, Hep3B and HL7702) was evaluated by western blot and FACS analysis. **(D-I)** Cytotoxic activity of GC33 CAR-T cells in response to the above six HCC cell lines, assessing at the indicated effector-to-target (E:T) ratios. **(J, K)** Mock, Ctrl CAR-T, or GC33 CAR-T cells were co-cultured in a 1:1 ratio with above six HCC cell lines. IL-2 and IFN γ content in the supernatant was determined by ELISA. All data were subjected to at least three separate experiments. Data were displayed as mean \pm SD. Unpaired Student's t-tests were employed for two-variable comparisons. One-way ANOVA was performed for multivariate comparisons. * $p < 0.05$; ** $p < 0.01$; *** $p < 0.001$; ns, no significance in comparison with control group

transduction efficiency differed little from each group (Fig. 1C and D). These results demonstrated that GC33 CAR-T cells were constructed successfully.

GC33 CAR T-cells display increased reactivity against GPC3-high tumor cells

To evaluate whether the GC33 CAR-T cell exhibited target-specific killing, we measured the GPC3 expression levels by western blot and flow cytometry in a panel of 6 HCC cell lines (HepG2, Huh7, SK-HEP-1, SMMC-7721, Hep3B, and HL7702). Among them, HepG2, Huh7 exhibited high GPC3 expression (Fig. 2A and C). We next assessed the effect of the GC33 CAR-T cell dose on the lytic activity against GPC3-high (HepG2 and Huh7), GPC3-middle (Hep3B and SMMC-7721) and GPC3-low (SK-HEP-1 and HL7702) HCC cell lines. GC33 CAR-T cells displayed a significantly increased lytic activity against GPC3-high HCC cell lines (Fig. 2D and I). In contrast, the cytotoxic potential of GC33 CAR-T cells in killing GPC3-cells was not significantly different from that of the control and mock group. In addition, against GPC3-high HCC cell lines, GC33 CAR-T cells were associated with higher production of proinflammatory cytokines IL-2 and IFN γ with respect to control CAR-T cells (Fig. 2J and K). However, there was little or no difference between the experimental and control group against GPC3-low HCC cell lines (Fig. 2H and I). The data suggested that GC33 CAR-T specifically recognized GPC3-expressing tumor cells and led to a strong killing effect.

Characteristics BSA-Len/PtNPs in vitro

The BSA-Len/PtNPs was prepared using previously established methods with slight modifications. Transmission electron microscopy (TEM) confirmed that the particles were approximately 5 nm in size (Fig. 3A). Molecular simulation and docking studies demonstrated that lenvatinib was effectively embedded within a specific pocket of Bovine Serum Albumin (BSA). Key interactions with amino acids such as ARG A:458, HIS A:145, LEU A:454, and ALA A:193 through hydrogen bonds, hydrophobic contacts, and van der Waals forces collectively stabilize lenvatinib within the BSA structure, thereby enhancing its solubility and potentially improving its therapeutic efficacy (Fig. 3B and C). To assess the O₂ generation capability of BSA-Len/PtNPs, the particles were resuspended in solutions with or without 10 mM H₂O₂, using Ru(dpp)₃Cl₂ as an O₂ fluorescence probe.

Fluorescence spectrophotometry revealed a significant decrease in fluorescence in the presence of H₂O₂, indicating efficient O₂ production (Fig. 3D and F). This suggests that PtNPs within the BSA-Len/PtNPs complex effectively catalyze the conversion of H₂O₂ into O₂, highlighting the potential of BSA-Len/PtNPs to generate oxygen in situ, which could be beneficial for therapeutic applications, particularly in hypoxic tumor environments.

BSA-Len/PtNPs promote vascular remodeling and alleviate hypoxia in HCC

Transforming disorganized, leaky tumor-associated vasculature into more structured, mature vessels has the potential to enhance therapeutic delivery and efficacy within the tumor microenvironment (Fig. 4A). To assess whether BSA-Len/PtNPs could contribute to vascular remodeling and alleviation of tumor hypoxia, three groups of NCG mice received treatment with three doses (0.04, 0.08 and 0.16 mg/kg/day) of saline, lenvatinib and BSA-Len/PtNPs at simultaneously from day 7 (7 days post 5×10^5 tumor cells in liver orthotopic implantation) to day 21 of the experiment, as indicated (Fig. 4B). Tumor volumes (one tumor per mouse) were monitored on day 7 and then weekly until all the mice reached the experimental endpoint. In line with previous reports, survival was significantly extended in mice treated with lenvatinib, especially in the BSA-Len/PtNPs group (Fig. 4C and E). Indeed, statistical differences were found among control, lenvatinib and BSA-Len/PtNPs low, medium and high dose groups (Fig. 4C and E). Notably, the longest overall survival of mice was found in BSA-Len/PtNPs group. Additionally, tissue sections were harvested from the liver following the sacrifice. Histopathological analysis was performed by immunohistochemistry to evaluate tumor vessel density (CD31 and α -SMA staining). It was observed that the tumor area was larger and the number of tumor angiogenesis was lower in the saline group (Fig. 4F). In contrast, in lenvatinib-treated (with or without delivery of nanozyme) groups, the tumor area was decreased, especially in the BSA-Len/PtNPs group (Fig. 4F). Notably, increased numbers of more aligned vessels with larger diameters were observed in the tumors of BSA-Len/PtNPs group (at the medium dose, but not the high dose group). These results implied that some notable striking vascular normalization persisted in the medium-dose BSA-Len/PtNPs group. These structural

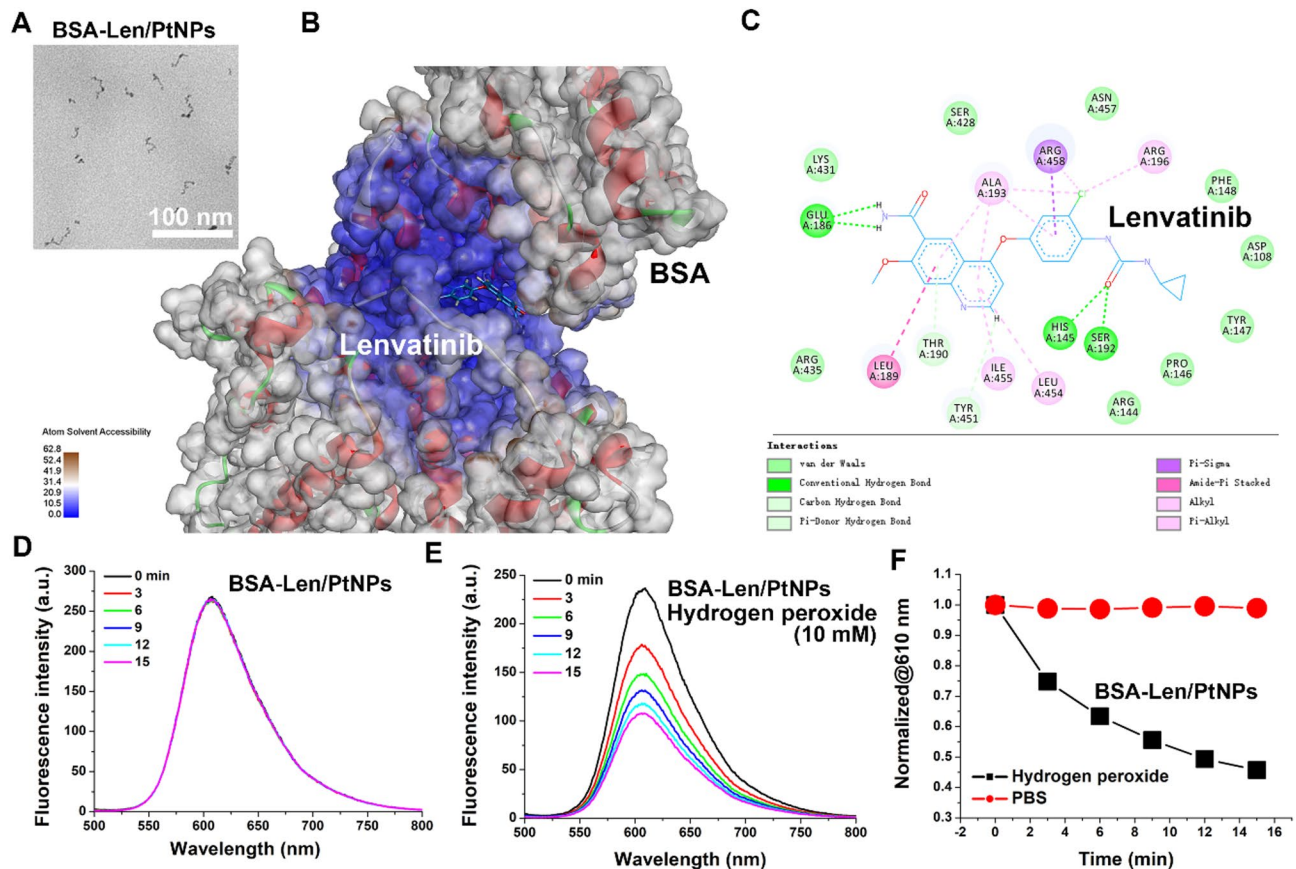


Fig. 3 Synthesis and Characterization of BSA-Len/PtNPs. (A) TEM image of BSA-Len/PtNPs. (B) and (C) Molecular simulation and docking studies of lenvatinib embed into the pocket of BSA. (D) and (E) Fluorescence spectra of Ru(dpp)₃Cl₂ in BSA-Len/PtNPs PBS solution with or without H₂O₂ (10 mM) at different incubation times. (F) Normalized fluorescence intensity of Ru(dpp)₃Cl₂ at 625 nm based on (D, E)

changes suggest potential improved vessel maturation and stabilization.

BSA-Len/PtNPs boosts GC33 CAR-T cell in vivo efficacy

To better assess whether the using of BSA-Len/PtNPs in combination with GC33 CAR-T cells has a synergistic effect and reduces drug resistance, we conducted further studies in immunocompromised NCG mice models. First, we established an orthotopic xenograft mouse model by implantation of 2×10^6 Huh7 cells into the liver of NCG mice. The tumor volume was monitored by bioluminescence on day 7 and the following each week. After detecting similar luciferase signals on day 7, tumor cells were treated with saline, lenvatinib, and BSA-Len/PtNPs (0.08 and 0.16 mg/kg/day) on day 8, and then GC33 CAR-T cells were administered on days 9 and 16 (Fig. 5A). We analyzed cancer progression in the “saline + CAR-T, lenvatinib + CAR-T, and BSA-Len/PtNPs + CAR-T” groups and revealed that cancer malignantly and rapidly progressed to day 21 in the only saline group, whereas CAR-T treatment slowed down tumor progression somewhat and prolonged survival to day 42 compared with saline group (Fig. 5B and C). In contrast,

both lenvatinib + CAR-T and BSA-Len/PtNPs + CAR-T groups exhibited inhibition of cancer growth, especially in the BSA-Len/PtNPs + CAR-T group (Fig. 5B and C). Interestingly, consistent with the previous results, the high-dose group currently used in the clinic did not show superiority over the medium-dose group (Fig. 5B and C). We assessed the expression of PD-1 on tumor-infiltrating CAR-T cells as a marker of exhaustion. PD-1 expression was significantly reduced in CAR-T cells from the BSA-Len/PtNPs treatment group compared to controls, suggesting a decrease in T cell exhaustion and potentially enhanced functional capacity within the tumor micro-environment (Figure S1). Our experimental results indicated that BSA-Len/PtNPs could synergize with CAR-T cells to kill tumor cells at a much lower dose by ameliorating hypoxia and promoting vascular normalization.

BSA-Len/PtNPs improve tumor oxygenation and enhance CAR-T cells infiltration

Based on these observations that the tumor vessel morphology was improved after being treated with BSA-Len/PtNPs, we next visualized the oxygenation of tumor tissues by tumor hypoxia markers HIF-1 α . The residual

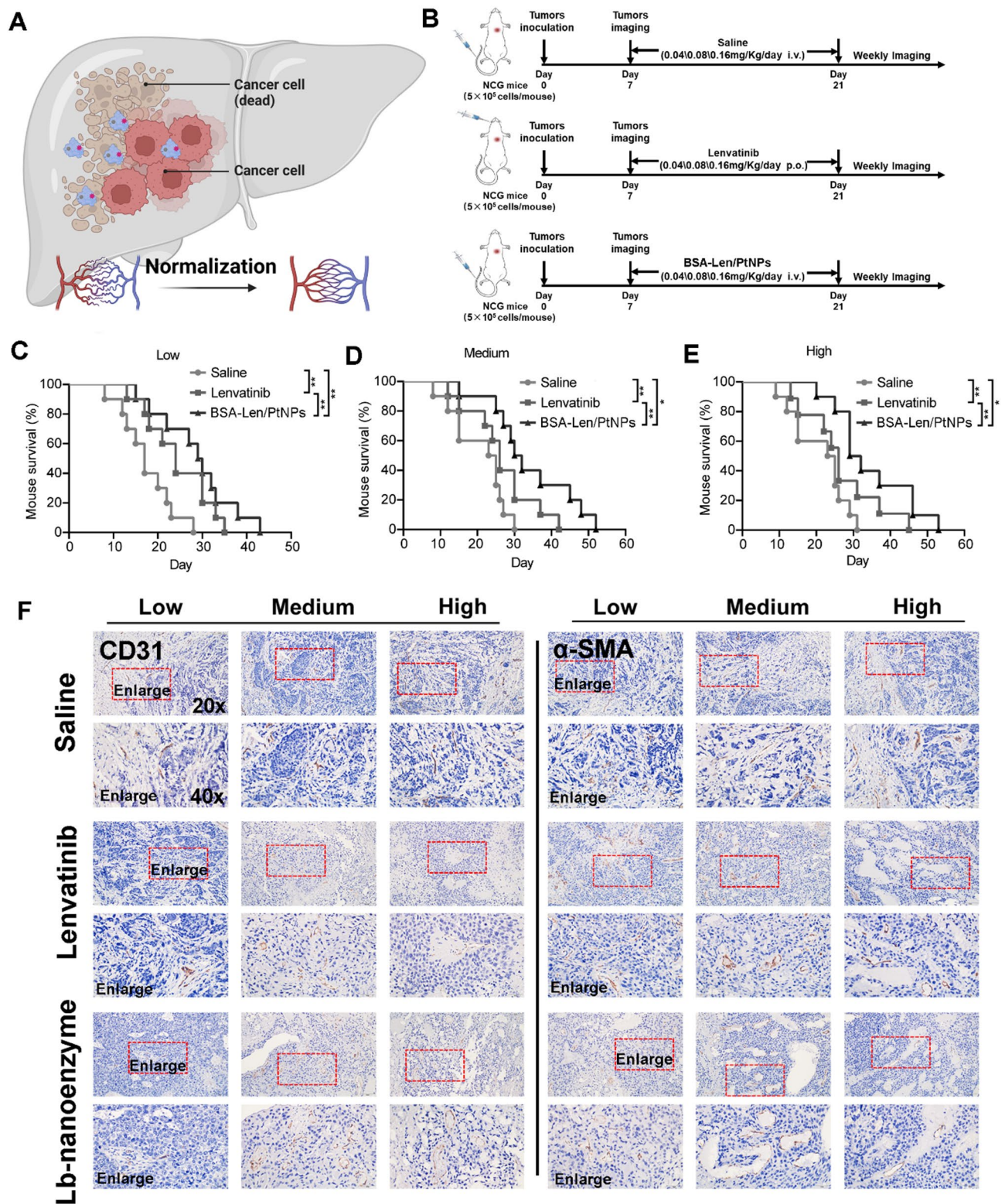


Fig. 4 Evaluating the impact of BSA-Len/PtNPs in vascular normalization in NCG Mice. **(A)** Schematic illustration of BSA-Len/PtNPs ameliorate hypoxia and normalize vessels of tumors in orthotopic HCC mice models. **(B)** Schematic diagram of the treatment of saline, lenvatinib and BSA-Len/PtNPs in the liver orthotopic implantation NCG mouse model. **(C-E)** Survival curves of mice in the various treatment groups. **(F)** Images of tumor tissue stained with CD31 and α-SMA. Original magnification, ×20 (insets); enlarged magnification, ×40 (insets). Log-rank method and Mann–Whitney U test were employed. * $p < 0.05$, ** $p < 0.01$, *** $p < 0.001$; ns, no significance in comparison with control group

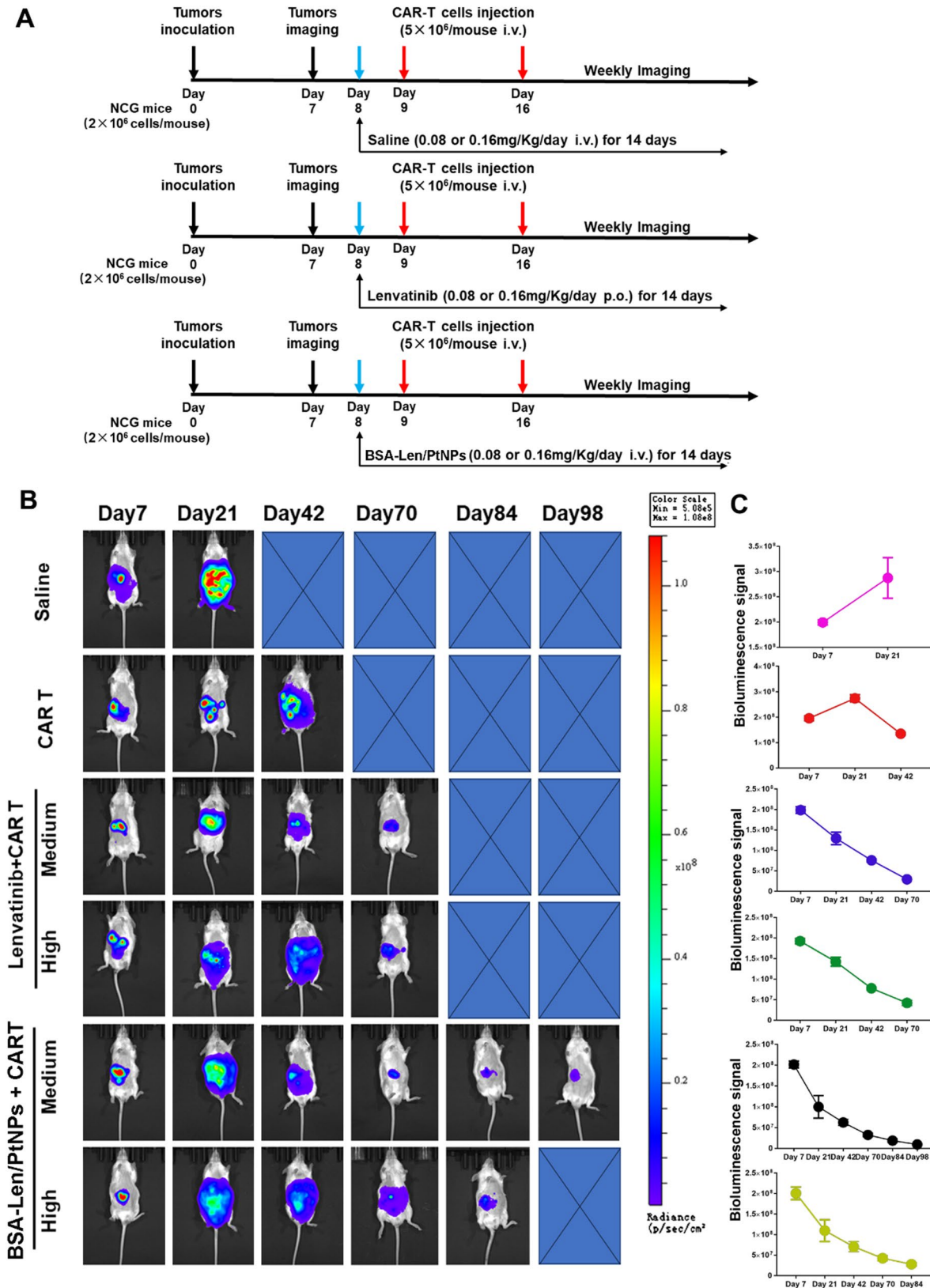


Fig. 5 BSA-Len/PtNPs enhance the effectiveness of GC33 CAR-T cells in vivo. **(A)** Schematic of the orthotopic mouse model in which NCG mice were systemically engrafted with luc-eGFP labeled Huh7 cells (2×10^6 cells), and treated with CAR-T cells plus two doses of saline/lenvatinib/BSA-Len/PtNPs (0.08 and 0.16 mg/kg/day), respectively. **(B)** Representative tumor BLI images at selected time points post-tumor inoculation. **(C)** Total flux intensity of orthotopic tumor BLI images at different time points after receiving various treatments as indicated ($n = 5$)

tumor tissues after treatment with the combination of lenvatinib and GC33 CAR-T cells had high HIF-1 α protein levels. By contrast, a low HIF-1 α expression level was detected in the BSA-Len/PtNPs+GC33 CAR-T cells group (Fig. 6A). As expected, no major differences in CAR-T cell infiltration were observed between saline+CAR-T and lenvatinib+CAR-T groups; whereas CAR-T cells were significantly enriched in BSA-Len/PtNPs+CAR-T group. This enrichment was more pronounced in the medium-dose group (Fig. 6B). Additionally, TUNEL staining results revealed a significant increase in TUNEL-positive cells in all three treatment groups compared to the saline group, and the BSA-Len/PtNPs+CAR-T exhibited the highest ratio of apoptosis cell (Fig. 6C and E). Interestingly, apoptosis cells in the high-dose group were 10% smaller than those in the medium-dose group (Fig. 6C and E). Taken together, these data substantiated the crucial role of BSA-Len/PtNPs in ameliorating tumor hypoxia and facilitating the infiltration and function of CAR-T cells.

Discussion

Previous studies have highlighted the difficulties of using CAR-T cells against solid tumors due to the hostile tumor microenvironment (TME), characterized by hypoxia, immunosuppressive factors, and abnormal tumor vasculature [34–36]. Traditional approaches, such as the direct modification of CAR-T cells or the combination with checkpoint inhibitors, have shown limited success in overcoming these barriers [37, 38]. Our study offers a comprehensive analysis of an innovative approach to enhance the efficacy of CAR-T cell therapy for hepatocellular carcinoma (HCC) by utilizing BSA-Len/PtNPs nanoparticles. We discovered that GC33 CAR-T cells, specifically engineered to target GPC3, effectively eliminate tumor cells with high GPC3 expression while demonstrating limited cytotoxicity against GPC3-low cancer cells. This high specificity is crucial for minimizing off-target effects on normal tissues, underscoring the potential of GC33 CAR-T cells in treating GPC3-positive HCC tumors. Furthermore, the development of BSA-Len/PtNPs holds significant promise in addressing challenges associated with hypoxia and abnormal tumor vasculature, common obstacles that often limit the effectiveness of CAR-T cell therapy in solid tumors. The BSA-Len/PtNPs were formulated by incorporating lenvatinib into BSA, stabilizing it through hydrogen bonding, hydrophobic interactions, and van der Waals forces with essential amino acids in BSA. This integration not only enhances lenvatinib's solubility but also improves its delivery to the tumor site, thereby increasing its therapeutic efficacy.

In vivo experiments demonstrated that BSA-Len/PtNPs effectively catalyzed the conversion of H₂O₂ into

O₂, generating oxygen that alleviates tumor hypoxia, which may offer a more balanced approach, promoting vessel normalization without exacerbating hypoxia. We observed that BSA-Len/PtNPs promote vascular normalization, further facilitating GC33CAR-T cell penetration and distribution throughout the tumor. When administered alongside GC33 CAR-T cells, BSA-Len/PtNPs markedly improved antitumor efficacy, especially at medium doses of the nanoparticles. This combination not only slowed tumor progression but also extended survival in mouse models, indicating a synergistic effect between the nanoenzyme and CAR-T cell therapy.

We sincerely appreciate the reviewer's insightful question regarding the observed superior efficacy of the medium-dose BSA-Len/PtNPs compared to the high-dose group. High-dose nanoparticles may elicit off-target toxicity through excessive reactive oxygen species (ROS) generation and accelerated clearance by the reticuloendothelial system (RES) [39]. Furthermore, supraphysiological concentrations of nanoparticles can drive aggregation via interparticle interactions, compromising colloidal stability and disrupting controlled drug release kinetics. Albumin-coated formulations (e.g., BSA-PtNPs) may lose their stealth properties under such conditions, leading to premature drug leakage and reduced tumor-targeting efficiency [40]. Concurrently, tumor cells exposed to high-dose cytotoxic agents often activate adaptive stress responses, such as PI3K/AKT signaling or autophagy, to evade apoptosis [41]. These interconnected mechanisms underscore the delicate balance required to optimize nanomedicine dosing for maximal efficacy while mitigating dose-limiting toxicity and adaptive resistance.

Additionally, our findings showed that BSA-Len/PtNPs enhanced tumor oxygenation and increased CAR-T cell infiltration, resulting in greater tumor cell apoptosis. The reduced expression of the hypoxia marker HIF-1 α and promoted vessel normalization in the combination of BSA-Len/PtNPs and CAR-T group further supports the bidirectional role of the nanoenzyme for enhancing the effectiveness of CAR-T cell therapy.

In summary, the findings of this study indicate that BSA-Len/PtNPs represent a promising adjunct to CAR-T cell therapy, particularly for solid tumors such as HCC, where hypoxia and abnormal vasculature present challenges. By leveraging nanotechnology to modulate the TME, particularly through oxygen generation and vascular normalization, BSA-Len/PtNPs not only facilitate improved infiltration and activity of CAR-T cells but also lead to better overall treatment outcomes. This approach may offer a potentially effective strategy for overcoming the limitations of current CAR-T cell therapies in solid tumors.

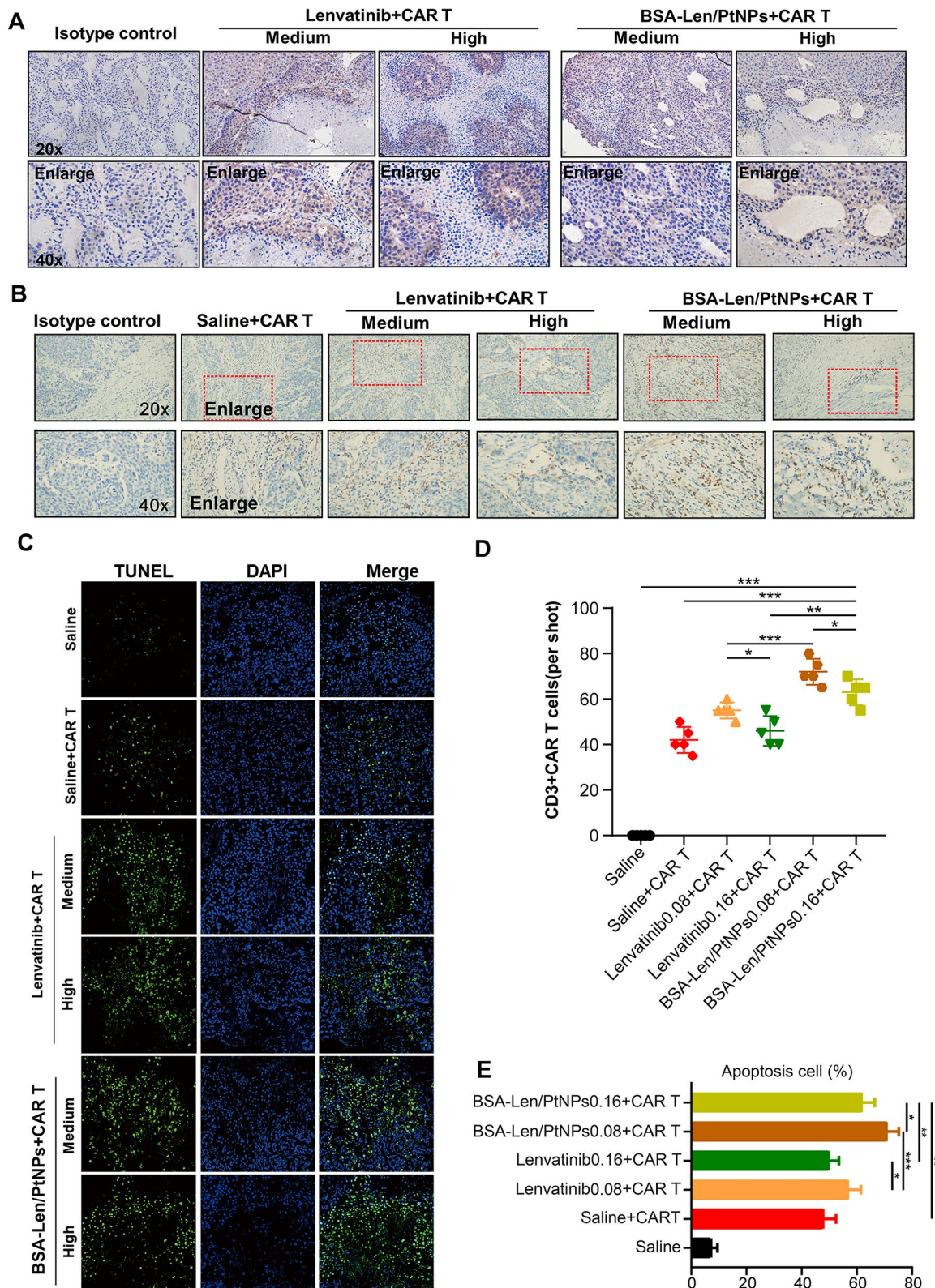


Fig. 6 BSA-Len/PtNPs reduce tumor hypoxia and boost CAR-T cell activity. **(A)** Representative immunohistochemical analysis of HIF-1 α expression in tumor tissue of the NCG mice from different groups. Original magnification, $\times 20$ (insets); enlarged magnification, $\times 40$ (insets). **(B)** IHC staining of paraffin tumor sections showed CAR T-cell infiltration. **(C)** Immunofluorescent staining against TUNEL was performed in tumor tissue of different treatment groups. Scale bar, 50 μ m. **(D)** Quantification of B. **(E)** Quantification of C. For all panels, data were obtained from at least 5 mice or 3 independent experiments, * $P < 0.05$, ** $P < 0.01$, *** $P < 0.001$, One-way ANOVA

Conclusions

This study demonstrates that the albumin-based nanoenzyme Lenv@BSA-PtNPs effectively addresses two critical barriers to CAR-T cell efficacy in solid tumors: hypoxia and abnormal vasculature. By catalyzing the conversion of H₂O₂ to O₂, the nanoenzyme ameliorates hypoxia in the tumor microenvironment (TME), downregulating HIF-1 α expression and reducing immunosuppressive signals. Simultaneously, its lenvatinib component promotes tumor vascular normalization, enhancing CAR-T cell infiltration and distribution. The combination of Lenv@BSA-PtNPs with GPC3-CAR T cells achieved synergistic antitumor effects in orthotopic HCC models, significantly prolonging survival and reducing tumor burden. Notably, medium-dose nanozyme exhibited superior efficacy compared to high-dose regimens, likely due to optimized vascular remodeling and mitigated off-target toxicity. These findings highlight the potential of bidirectional nanoenzymes as a simple yet potent strategy to enhance adoptive cell therapies for solid tumors. Future studies should explore scalable formulations and validate this approach in immunocompetent models to advance clinical translation.

Limitations

Several limitations should be considered in this study. First, the use of NOD mice, which lack a functional adaptive immune system, precludes the evaluation of interactions between CAR-T cells and endogenous immune cell populations, such as Tregs and MDSCs. Thus, the broader effects of BSA-Len/PtNPs on the immune microenvironment remain unclear. Second, while we included saline + CAR-T and lenvatinib + CAR-T groups as controls, we did not incorporate additional formulations, such as BSA-PtNPs alone or lenvatinib encapsulated in nanoparticles without platinum, which would provide further insight into the contributions of each nanoenzyme component. Third, although measuring intratumoral blood-flow dynamics and ROS would have strengthened our mechanistic insights, current instrumentation and technical constraints precluded these assays, and their effects were inferred indirectly. Lastly, the long-term safety and pharmacokinetics of BSA-Len/PtNPs were not addressed here and should be explored in future studies. Further work in immunocompetent models and comprehensive pharmacological assessments will be essential for evaluating the full therapeutic potential of this approach.

Abbreviations

BSA	Bovine serum albumin
CAR	Chimeric antigen receptor
GPC3	Glypican-3
HCC	Hepatocellular carcinoma
HIF-1 α	Hypoxia-inducible factor 1-alpha
IL-2	Interleukin-2

IFN- γ	Interferon-gamma
NOD	Nonobese diabetic (mice)
NCG	NOD-Prkdcem26Cd52Il2rgem26Cd22/Nju (mice strain)
PtNPs	Platinum nanoparticles
PBMCs	Peripheral blood mononuclear cells
ROS	Reactive oxygen species
RES	Reticuloendothelial system
TME	Tumor microenvironment
TUNEL	Terminal deoxynucleotidyl transferase dUTP Nick-End Labeling
VEGF	Vascular endothelial growth factor

Supplementary Information

The online version contains supplementary material available at <https://doi.org/10.1186/s12967-025-06636-7>.

Supplementary Material 1

Acknowledgements

Not applicable.

Author contributions

Y. X., W. Z. and A. H. conceived and designed the study. Y. X., J. L. and J. W. conducted all experimental procedures, and performed statistical analyses of the data. Y. G. and Y. W. oversaw data visualization and experimental validation. M. G. and W. L. provided critical technical support. The manuscript was drafted by Y. X. All authors critically reviewed the manuscript, provided substantive feedback, and approved the final version for publication.

Funding

This project was supported by Startup Found for scientific research, Fujian Medical University (Grant number: 2022QH2004), the Foundation of the Finance Department of Fujian Province of China (Grant/Award Number: 21SCZZX002).

Data availability

The data used and/or analysed during the current study are available from the authors on reasonable request.

Declarations

Ethics approval and consent to participate

Animal experiments were conducted with the approval and oversight of the Institutional Committee for Animal Welfare. All animal experiments were approved and reviewed by Fujian Medical Experimental Animal Care Commission (FJMU IACUC2018-038).

Consent for publication

Not applicable.

Competing interests

The authors declare that they have no competing interests.

Received: 10 March 2025 / Accepted: 21 May 2025

Published online: 13 June 2025

References

- Schuster SJ, Svoboda J, Chong EA, Nasta SD, Mato AR, Anak O, Brogdon JL, Pruteanu-Malinici I, Bhoj V, Landsburg D, Wasik M, Levine BL, Lacey SF, Melenhorst JJ, Porter DL, June CH. Chimeric antigen receptor T cells in refractory B-Cell lymphomas. *N Engl J Med*. 2017;377(26):2545–54.
- Lu J, Jiang G. The journey of CAR-T therapy in hematological malignancies. *Mol Cancer*. 2022;21(1):194.
- Wang H, Kaur G, Sankin AI, Chen F, Guan F, Zang X. Immune checkpoint blockade and CAR-T cell therapy in hematologic malignancies. *J Hematol Oncol*. 2019;12(1):59.

4. Majzner RG, Mackall CL. Tumor antigen escape from CAR-T-cell therapy. *Cancer Discov.* 2018;8(10):1219–26.
5. Kumar C, Kohli S, Chiliveru S, Bapsy PP, Jain M, Suresh Attili VS, Mohan J, Vaid AK, Sharan B. A retrospective analysis comparing APCEDEn((R)) dendritic cell immunotherapy with best supportive care in refractory cancer. *Immunotherapy.* 2017;9(11):889–97.
6. Wu J, Yang S, Xu K, Ding C, Zhou Y, Fu X, Li Y, Deng M, Wang C, Liu X, Li L. Patterns and trends of liver Cancer incidence rates in Eastern and southeastern Asian countries (1983–2007) and predictions to 2030. *Gastroenterology.* 2018;154(6):1719–28. e5.
7. Newick K, O'Brien S, Moon E, Albelda SM. CART cell therapy for solid tumors. *Annu Rev Med.* 2017;68:139–52.
8. Liu Q, Li J, Zheng H, Yang S, Hua Y, Huang N, Kleff J, Liao Q, Wu W. Adoptive cellular immunotherapy for solid neoplasms beyond CAR-T. *Mol Cancer.* 2023;22(1):28.
9. Sun L, Gao F, Gao Z, Ao L, Li N, Ma S, et al. Shed antigen-induced blocking effect on CAR-T cells targeting glypican-3 in hepatocellular carcinoma. *J Immunother Cancer.* 2021;9(4):e001875.
10. Albelda SM. CAR T cell therapy for patients with solid tumours: key lessons to learn and unlearn. *Nat Rev Clin Oncol.* 2024;21(1):47–66.
11. Maalej KM, Merhi M, Inchakalody VP, Mestiri S, Alam M, Maccalli C, Cherif H, Uddin S, Steinhoff M, Marincola FM, Dermime S. CAR-cell therapy in the era of solid tumor treatment: current challenges and emerging therapeutic advances. *Mol Cancer.* 2023;22(1):20.
12. Chen Z, Han F, Du Y, Shi H, Zhou W. Hypoxic microenvironment in cancer: molecular mechanisms and therapeutic interventions. *Signal Transduct Target Ther.* 2023;8(1):70.
13. Wu Q, You L, Nepovimova E, Heger Z, Wu W, Kuca K, Adam V. Hypoxia-inducible factors: master regulators of hypoxic tumor immune escape. *J Hematol Oncol.* 2022;15(1):77.
14. Wu H, Zhao X, Hochrein SM, Eckstein M, Gubert GF, Knöpper K, Mansilla AM, Öner A, Doucet-Ladevèze R, Schmitz W, Ghesquière B, Theurich S, Dudek J, Gasteiger G, Zerneck A, Kobold S, Kastenmüller W, Vaeth M. Mitochondrial dysfunction promotes the transition of precursor to terminally exhausted T cells through HIF-1 α -mediated glycolytic reprogramming. *Nat Commun.* 2023;14(1):6858.
15. Barsoum IB, Smallwood CA, Siemens DR, Graham CH. A mechanism of hypoxia-mediated escape from adaptive immunity in cancer cells. *Cancer Res.* 2014;74(3):665–74.
16. Bailey CM, Liu Y, Liu M, Du X, Devenport M, Zheng P, et al. Targeting HIF-1 α abrogates PD-L1-mediated immune evasion in tumor microenvironment but promotes tolerance in normal tissues. *J Clin Invest.* 2022;132(9):e150846.
17. Li G, Du R, Wang D, Zhang X, Wang L, Pu S, et al. Improved efficacy of triple-negative breast cancer immunotherapy via hydrogel-based co-delivery of CAR-T cells and mitophagy agonist. *Adv Sci (Weinh).* 2025;12(14):e2409835.
18. Dong X, Ren J, Amoozgar Z, Lee S, Datta M, Roberge S, et al. Anti-VEGF therapy improves EGFR-vIII-CAR-T cell delivery and efficacy in syngeneic glioblastoma models in mice. *J Immunother Cancer.* 2023;11(3):e005583.
19. Zeng W, Yu M, Chen T, Liu Y, Yi Y, Huang C, Tang J, Li H, Ou M, Wang T, Wu M, Mei L. Polypyrrole nanoenzymes as tumor microenvironment modulators to reprogram macrophage and potentiate immunotherapy. *Adv Sci (Weinh).* 2022;9(23):e2201703.
20. Lyu M, Zhu D, Kong X, Yang Y, Ding S, Zhou Y, Quan H, Duo Y, Bao Z. Glutathione-Depleting nanoenzyme and glucose oxidase combination for hypoxia modulation and radiotherapy enhancement. *Adv Healthc Mater.* 2020;9(11):e1901819.
21. Xie P, Zhang L, Shen H, Wu H, Zhao J, Wang S, Hu L. Biodegradable MoSe(2)-polyvinylpyrrolidone nanoparticles with multi-enzyme activity for ameliorating acute pancreatitis. *J Nanobiotechnol.* 2022;20(1):113.
22. Zeng Z, Zhang C, Li J, Cui D, Jiang Y, Pu K. Activatable polymer nanoenzymes for photodynamic immunometabolic Cancer therapy. *Adv Mater.* 2021;33(4):e2007247.
23. Ansari SA, Husain Q. Potential applications of enzymes immobilized on/in nano materials: A review. *Biotechnol Adv.* 2012;30(3):512–23.
24. Ashrafi AM, Bytesnikova Z, Barek J, Richtera L, Adam V. A critical comparison of natural enzymes and nanozymes in biosensing and bioassays. *Biosens Bioelectron.* 2021;192:113494.
25. Manea F, Houillon FB, Pasquato L, Scrimin P. Nanozymes: gold-nanoparticle-based transphosphorylation catalysts, angewandte chemie. English). 2004;43(45):6165–9.
26. Mehta D, Singh S. Nanozymes and their biomolecular conjugates as next-generation antibacterial agents: A comprehensive review. *Int J Biol Macromol.* 2024;278Pt 1:134582.
27. Zhang A, Gao A, Zhou C, Xue C, Zhang Q, Fuente JM, Cui D. Confining prepared ultrasmall nanozymes loading ATO for lung Cancer catalytic therapy/immunotherapy. *Adv Mater.* 2023;35(45):e2303722.
28. Li D, Ha E, Zhou Z, Zhang J, Zhu Y, Ai F, Yan L, He S, Li L, Hu J. Spark PtMnIr nanozymes for Electrodynamic-Boosted multienzymatic tumor immunotherapy. *Adv Mater.* 2024;36(13):e2308747.
29. Chen Q, Liu Z. Albumin carriers for Cancer theranostics: A conventional platform with new promise. *Adv Mater.* 2016;28(47):10557–66.
30. Lan S, Lin Z, Zhang D, Zeng Y, Liu X. Photocatalysis enhancement for programmable killing of hepatocellular carcinoma through Self-Compensation mechanisms based on black phosphorus Quantum-Dot-Hybridized nano-catalysts. *ACS Appl Mater Interfaces.* 2019;11(10):9804–13.
31. Capurro M, Wanless IR, Sherman M, Deboer G, Shi W, Miyoshi E, Filmus J. Glypican-3: a novel serum and histochemical marker for hepatocellular carcinoma. *Gastroenterology.* 2003;125(1):89–97.
32. Batra SA, Rathi P, Guo L, Courtney AN, Fleurence J, Balzeau J, Shaik RS, Nguyen TP, Wu MF, Bulsara S, Mamonkin M, Metelitsa LS, Heczey A. Glypican-3-Specific CAR T cells coexpressing IL15 and IL21 have superior expansion and antitumor activity against hepatocellular carcinoma. *Cancer Immunol Res.* 2020;8(3):309–20.
33. Jiang Z, Jiang X, Chen S, Lai Y, Wei X, Li B, Lin S, Wang S, Wu Q, Liang Q, Liu Q, Peng M, Yu F, Weng J, Du X, Pei D, Liu P, Yao Y, Xue P, Li P. Anti-GPC3-CAR T cells suppress the growth of tumor cells in Patient-Derived xenografts of hepatocellular carcinoma. *Front Immunol.* 2016;7:690.
34. Zhang ZZ, Wang T, Wang XF, Zhang YQ, Song SX, Ma CQ. Improving the ability of CAR-T cells to hit solid tumors: challenges and strategies. *Pharmacol Res.* 2022;175:106036.
35. Flugel CL, Majzner RG, Krenciute G, Dotti G, Riddell SR, Wagner DL, Abou-El-Enen, overcoming on-target, off-tumour toxicity of CAR T cell therapy for solid tumours. *Nat Rev Clin Oncol.* 2023;20(1):49–62.
36. Sterner RC, Sterner RM. CAR-T cell therapy: current limitations and potential strategies. *Blood cancer J.* 2021;11(4):69.
37. Grosser R, Cherkassky L, Chintala N, Adusumilli PS. Combination immunotherapy with CAR T cells and checkpoint Blockade for the treatment of solid tumors. *Cancer Cell.* 2019;36(5):471–82.
38. Majzner RG, Theruvath JL, Nellan A, Heitzeneder S, Cui Y, Mount CW, Rietberg SP, Linde MH, Xu P, Rota C, Sotillo E, Labanieh L, Lee DW, Orentas RJ, Dimitrov DS, Zhu Z, Croix BS, Delaidelli A, Sekunova A, Bonvini E, Mitra SS, Quezado MM, Majeti R, Monje M, Sorensen PHB, Maris JM. Mackall, CAR T cells targeting B7-H3, a Pan-Cancer antigen, demonstrate potent preclinical activity against pediatric solid tumors and brain tumors. *Clin Cancer Research: Official J Am Association Cancer Res.* 2019;25(8):2560–74.
39. Pedone D, Moglianetti M, De Luca E, Bardi G, Pompa PP. Platinum nanoparticles in nanobiomedicine. *Chem Soc Rev.* 2017;46(16):4951–75.
40. Hashimoto M, Sasaki JI, Yamaguchi S, Kawai K, Kawakami H, Iwasaki Y, Imazato S. Gold nanoparticles inhibit matrix metalloproteases without cytotoxicity. *J Dent Res.* 2015;94(8):1085–91.
41. Faderin E, Iorkula TH, Aworinde OR, Awoyemi RF, Awoyemi CT, Acheampong E, Chukwu JU, Agyemang P, Onaiwu GE, Ifjen IH. Platinum nanoparticles in cancer therapy: chemotherapeutic enhancement and ROS generation. *Med Oncol.* 2025;42(2):42.

Publisher's note

Springer Nature remains neutral with regard to jurisdictional claims in published maps and institutional affiliations.